



A Prospect for Environmental Remediation of Perchlorate via Cost-Effective Pinus Leaves and Dandelion Flower Powder-based Layer Double Hydride (LDH) Sorbents

Ammara Ahmed^a, Addison Francis^a, Na Liu^{a,*}, Ying Ying Liu^{b,**}

^a Key Laboratory of Groundwater Resources and Environment, Ministry of Education, College of Environment and Resources, Jilin University, Changchun 130021, China

^b Department of Earth and Environmental Science, University of Waterloo, Ontario N2L3G1, Canada

Received 10 December 2019; accepted 9 February 2020

Available online 18 March 2020

KEYWORDS

LDHs;
PiP-LDH;
DFP-LDH;
Adsorptive removal

Abstract In this study, pine leaves powder (PiP) and dandelion flower powder (DFP) were repurposed to synthesize layered double hydroxides (LDHs) to form a base for sorbents used in perchlorate remediation from wastewater. The effects of the adsorbent dose, pH, thermodynamics, and coexisting ions were evaluated in batch experiments. The results revealed that 0.1 g adsorbent (PiP-LDH and DFP-LDH) removed 97% and 93% of perchlorate contaminants, respectively. In this study, the correlation coefficient of pseudo-second-order was higher than pseudo-first-order for all the LDHs. The kinetic and isotherm studies showed the best uptake of perchlorate in the short time was by PiP-LDH, followed by DFP-LDH (20 min and 40 min, respectively). The calculated and experimental values of adsorption at the equilibrium state also concurred with the pseudo-second-order model. The prepared LDHs were mesoporous. The surface area of PiP-LDH provided more adsorption sites, rendering it more suitable for perchlorate adsorption compared with the other two LDHs. The model suggests Physico-chemical interactions behind the sorption of perchlorate by LDHs. The adsorption was more influenced by anions i.e. $\text{PO}_4^{3-} > \text{SO}_4^{2-} > \text{NO}_3^-$ than monovalent anions due to the increase in the charge radius values. The prepared LDHs could be of great benefit to the environmental remediation of wastewater bodies.

© 2020 The Authors. Published by Elsevier B.V. on behalf of King Saud University. This is an open access article under the CC BY-NC-ND license (<http://creativecommons.org/licenses/by-nc-nd/4.0/>).

* Corresponding author.

** Corresponding author.

E-mail addresses: liuna@jlu.edu.cn (N. Liu), yy4liu@uwaterloo.ca (Y.Y. Liu).

Peer review under responsibility of King Saud University.



1. Introduction

Perchlorate, which is inorganic, is a potable water contaminant. Perchlorate contamination has been found in potable water across the world (Lin et al., 2014; US EPA, 2014). Perchlorate ions are undesirable in the environment because of their toxicity to humans (Darracq et al., 2014). In 1998,

perchlorate was added to the Contaminant Candidate List for water (EPA, 1998), which means the chemical needs evaluating to determine its potential hazard as significant environmental contamination and requires regulating (Wagner et al., 2017; Wendelken et al., 2006). Perchlorate exists as an anion component in salts, including potassium, ammonium, sodium, and perchloric acid. They are widespread in the environment, such as in soil, ground, and surface water, and vegetation (Srinivasan and Thiruvengatachari, 2009). Ammonium perchlorate is an oxidant used in the production of firearms and rocket engines. Chile saltpeter, used in fertilizers, contains traces of perchlorate. However, agricultural use does not account for the widespread contamination (Gullick et al., 2001; Urbansky, 2002). The Chilean caliche deposits are a natural source of perchlorate in underground water bodies; however, other sources of anthropogenic origin should not be overlooked and contribute more than natural sources (US EPA, 2014).

The presence of perchlorate in water is a public health concern because it inhibits the uptake of iodine by the thyroid (Titulaer et al., 1994). Perchlorate-related toxicity may result in nervous system defects, thyroid dysfunction, and many other problems in people exposed to the contaminant (Chen et al., 2005). Perchlorate, when reduced to chlorite and chlorate, induced hemolytic anemia and the formation of methemoglobin in exposed lab animals. It is also toxic to plants and microorganisms (Chen et al., 2005; Wilkin et al., 2007). The oral reference dose (RfD) assigned by USEPA equals $0.0007 \text{ mg kg}^{-1}$ of body weight/day or $0.7 \text{ }\mu\text{g/kg/day}$ (EPA IRIS 2005), which is equivalent to a level of 24.5 ppb perchlorate in drinking water (USEPA, 2003).

Several techniques are currently used for the remediation and removal of perchlorate from contaminated sites (US EPA, 2014; Darracq et al., 2014). Materials used for remediation include the following: granular activated carbon, granular ferric hydroxide, cross-linked Fe (III)-chitosan, rice husk composites with MCM-48, and organosilica and acid-washed, zero-valent aluminum along with aluminum hydroxide, using Protonated cross-linked chitosan. Several processes such as reverse osmosis, electro dialysis, ultrafiltration, and chemical and electrochemical reduction, are used. However, some of these methods have limited application, as they are costly and non-selective (Bardiya and Bae et al., 2011). LDHs are among a class of compounds that are lamellar, ionic, and have positively charged brucite-like layers. They are currently of increasing research interest, for having interlayer containing charge-compensating anions (Wang and O'Hare, 2012; Debdipta et al., 2014). However, several studies reporting LDH-based adsorption used harmful chemicals such as arsenate, chromate, and phosphate, and also had some limitations, e.g., longer equilibrium time and using a higher concentration of adsorbent (Park and Kim, 2011; Debdipta et al., 2014).

This study evaluated the efficacy of perchlorate sorption using newly synthesized LDHs. The LDHs were repurposed as biochemical sorbents using pine leaves powder (PiP-LDH) and dandelion flower powder (DFP-LDH). The percentage of sorption was studied with time, temperature, pH, and thermodynamics. Finally, using the data regarding the parameters mentioned above, the study aimed to establish the optimum conditions to maximize the sorption of perchlorate anions using the smallest amount of LDHs, in the quickest possible time.

2. Materials and methods

2.1. Chemicals and reagents

The chemicals used in the analytical procedures, purchased from Sigma Aldrich, were of high purity and analytical grade. The list includes hydrate sodium perchlorate ($\text{NaClO}_4 \cdot \text{H}_2\text{O}$), magnesium nitrate hexahydrate ($\text{Mg}(\text{NO}_3)_2 \cdot 6\text{H}_2\text{O}$), aluminum nitrate nonahydrate ($\text{Al}(\text{NO}_3)_3 \cdot 9\text{H}_2\text{O}$), hydrochloric acid (HCl) and sodium hydroxide (NaOH).

2.2. Preparation of pinus leaf powder (PiP) and the dandelion flowers powder (DFP)

We collected the pine leaves (*Pinus strobus*) and dandelion flowers from the university lawn into plastic bags. The obtained leaves were thoroughly washed with ultrapure water to remove dirt, debris, and other adhering impurities from their surface. The pine leaves were dried in an oven for 72 h at $70 \text{ }^\circ\text{C}$ to remove additional moisture. Then the dried leaves were pulverized into a fine powder using a mixer and grinder and were then passed through a molecular sieve of 100 mesh size (0.5 mm). The dandelion flowers were also washed with ultrapure water and were dried at a temperature of $70 \text{ }^\circ\text{C}$ for 24 h. The dried flowers were ground into a fine powder, using a manually operated mortar, and then sieved via of 100 mesh size (0.5 mm) sieves.

2.3. Mechano-chemical synthesis of LDHs

2.3.1. Dry grinding

In this study, nitrate-based-LDH (N-LDH, Mg-Al-NO_3) was used as a parent LDH, to compare its effectiveness with newly modified LDHs. The N-LDH was synthesized mechano-chemically following a dry grinding procedure. PiP-LDH was prepared in a manual mortar using the pulverized magnesium nitrate, aluminum nitrates, and PiP in the ratio 2:3:2, the added 3.4gs of NaOH. The mixture was then thoroughly ground for 15 min until it developed a sticky paste-like consistency. The paste was washed with 20 mL ultrapure water four times, using pump filtration. The resulting mixtures of LDHs were vacuum-dried overnight at $40 \text{ }^\circ\text{C}$. The DFP-LDH was prepared using the same method.

2.4. Structural characterization of prepared LDHs

The morphological characteristics of LDHs were analyzed under a scanning electron microscope (SEM) (Merlin, compact ZEISS 1550VP) operated at 25 kV. The X-ray photoelectron spectroscopy (XPS) (Escalab 250, Thermo Fisher, USA) was operated using an Escalab 250-spectrometer equipped with the Al-K-Alpha (1486.6 eV), $500 \text{ }\mu\text{m}$ [15 kV150 W]. The analysis was extended to visualize the surface to provide useful information on the chemical state of the material's surface. X-ray diffraction (Shimadzu DX-2700) was employed to determine the crystallography structure and orientation of the LDH materials. The operational conditions optimized for the analysis were 40 kV and 30 mA with radiation CuK α at a scanning rate of 0.12 s. The surface area was also calculated through nitrogen adsorption/desorption using a Brunauer–Emmett–

Teller (BET) instrument (Tristar, Micromeritics, ASAP 2010N analyzer). The instrument was optimized at $-196\text{ }^{\circ}\text{C}$, and the sample mass was 0.1 g. Furthermore, the amount of nitrogen absorbed was measured to evaluate the pore volume. The Barrett–Joyner–Halenda model was used to calculate the average pore size distribution. Fourier transform infrared spectroscopy (FTIR) (Nexus 670, Nicolet, USA) was also used to identify functional groups and vibration changes pre- and post-adsorption by the prepared LDHs.

2.5. Determining the LDH's point of zero charges (pHpzc)

The point of zero charges (i.e., pHpzc) was determined using the pH drift method. The method was based on 0.01 g powdered LDHs and 100 mL of 0.01 M NaCl solution (with varying pH values ranging between 3 and 12). The mixture is taken in conical flasks, followed by shaking for 24 h, and the pH measured at the final stage was plotted against the initial pH values. The pHpzc is the point of the curve at which the initial pH equals the final pH (Srivastava et al., 2011).

2.6. The batch experiment

The batch experiment was performed in triplicate to ensure the concurrency of the results. A stock solution of 1 gL^{-1} perchlorate was prepared with sodium perchlorate and was preserved at $4\text{ }^{\circ}\text{C}$ for further dilution to prepare working solutions. The sample solutions prepared for the kinetic study were of 100 mgL^{-1} strength, containing 100 mg adsorbent (i.e. representing ~ 10 times the perchlorate concentration in the environment). The solutions were poured into a horizontal shaker operated at 200 rpm at a constant temperature of $30\text{ }^{\circ}\text{C}$. The run times selected for the kinetic study ranged between 5 min and 24 h. The resulting supernatant solution was centrifuged at 15,000 rpm for 5 min and filtered through micro syringe filtration of $0.45\text{ }\mu\text{m}$. The isotherm study was conducted using concentrations ranging between 2 mgL^{-1} and 500 mgL^{-1} . The Isotherm was conducted with a range of concentrations, to test the maximum adsorption capacity of the given material at given temperature time and adsorbent amount. Additionally, the process of adsorption was also tested with varying parameters, including different ranges of pH (between 3 and 12), temperature (between 20 and $50\text{ }^{\circ}\text{C}$), thermodynamic study, and the effect of coexisting ions.

2.7. Analysis of perchlorate-ion chromatography

The perchlorate contents in the samples were analyzed using ion chromatography (Dionex ICS 2100) equipped with an AS-20 and AG-20 guard column. The instrument was equipped with a suppressed conductivity detector and was optimized at $30\text{ }^{\circ}\text{C}$, 87 mA, and 35 Mm potassium hydroxide was used as an eluent. The injection volume of the samples was $200\text{ }\mu\text{L}$.

2.8. Kinetic study and isotherm study

The kinetic models were further employed to evaluate the interaction mechanism, kinetic parameters and sorption kinet-

ics of perchlorate on LDHs. Linear models and equations were employed:

Pseudo-first-order kinetic model:

$$\ln(q_e - q_t) = \ln q_e - k_1 t \quad (1)$$

where \ln represent log.

Pseudo-second-order kinetic model:

$$t/q_t = 1/k_2 q_e^2 + t/q_e \quad (2)$$

where the q_e and q_t (mgg^{-1}) represent the amount of perchlorate sorbed at an equilibrium stage and at any time, respectively. Likewise, the k_1 (min^{-1}) and k_2 ($\text{g}^{-1}\text{ mg}^{-1}\text{ min}^{-1}$) represents the pseudo-first-order and pseudo-second-order constants, respectively.

On the other hand, the intra-particle diffusion model is described below:

$$q_t = k_i t^{0.5} + C_i$$

where k_i ($\text{mgg}^{-1}\text{ min}^{0.5}$) is the intra-particle diffusion rate constant for stage i and C_i is the intercept of stage i describing the boundary layer effect in the external diffusion.

The amount of perchlorate adsorbed, q_e (mgg^{-1}), by the LDH adsorbents at equilibrium state was calculated using the following equation:

$$q_e(\text{mgg}^{-1}) = (C_i - C_t) \times V/1000 \times M \quad (3)$$

where ' C ' represents the concentration (mgL^{-1}) at the initial stage (C_i) or at any specified time (C_t), the volume, ' V ' (ml), represents the perchlorate solution used in this study, and the ' M ' denotes the mass (g) of LDH adsorbent.

Furthermore, two isotherm models (Langmuir and Freundlich) were also considered to estimate the trends in the equilibrium adsorption data and fit the experimental data of adsorption. The models are as follows:

$$q_e = q_{\max} K_L C_e / (1 + K_L C_e) \text{ (Langmuir isotherm model)} \quad (4)$$

$$q_e = K_f \times C_e^{1/n} \text{ (Freundlich isotherm model)} \quad (5)$$

where C_e is the perchlorate concentration at the given equilibrium state, q_{\max} represents the capacity of sorption, and K_L is the Langmuir constant (L mmol^{-1}) of sorption equilibrium, while ' n ' and K_f are the Freundlich constants, on the intensity and capacity of adsorption, respectively.

2.9. Thermodynamics

The thermodynamics of an adsorption process is also worth considering for assessing whether the process is spontaneous or not. Gibb's free energy change (ΔG°) is the fundamental criterion of spontaneity. Reactions occur spontaneously at a given temperature if the ΔG° bears a negative value. The thermodynamic parameters of Gibb's free energy change include the enthalpy change (ΔH°) and entropy change (ΔS°) for the adsorption processes were calculated using the following equations:

$$\Delta G = -RT \ln K_L$$

$$\Delta G = \Delta H^{\circ} - T \Delta S^{\circ}$$

where R is the universal gas constant ($8.314\text{ J mol}^{-1}\text{ K}^{-1}$), and T is the absolute temperature taken in Kelvin (K).

$$K_L = q_{\max} \times B$$

K_L was obtained from the Langmuir isotherm, while the enthalpy change, ΔH° , and the entropy change, ΔS° , were obtained from the intercept and slope of plot $\ln K_L$ for the adsorption processes, versus temperature, $1/T$ (Fig. S8). The negative values of ΔG° confirm the feasibility of the process and the spontaneous nature of adsorption. The positive value of ΔH° indicates that the adsorption reaction is endothermic. The positive change in entropy ΔS° suggests likely structural changes that occurred on the adsorbent, and the randomness at the solid-liquid interface in the adsorption system increased during the adsorption process (Table 2).

3. Results and discussion

3.1. LDH's structure characterization using BET- N_2 , XRD, XPS, and FTIR-spectra

To our knowledge, this is the first study to report the efficacy of perchlorate sorption using PiP- and DFP-based LDHs. The LDHs were of H-V-type isotherm at slightly high pressure (between 0.5 and 1.0 bar) Fig. S1, while the BET analysis suggested the mesoporous qualities of the LDHs. The IUPAC classification was suggestive of LDH's mesoporous structure with a pore size between 2 and 50 nm (Rouquerol et al., 1994; see Supplementary Table S1). In this study, the BET- N_2 surface areas of the PiP, DFP, and N-LDH were $4.5 \text{ m}^2 \text{ g}^{-1}$, $4.8 \text{ m}^2 \text{ g}^{-1}$, and $16.7 \text{ m}^2 \text{ g}^{-1}$, respectively. As PiP-LDH had the smallest surface area, indicating a considerable pore density distribution on PiP-LDH's surface, providing more active sites for adsorption compared to other LDHs. The current results were better than a previous study (Yu et al., 2009), reporting the smallest surface of current adsorbent than alumina, silica, and zeolite, anion exchange resin, and powder activated carbon. Since the smaller surface area and pore size did not cause pore blockage, and the steric hindrance of perchlorate was less evident in small size adsorbent (Deng et al., 2010).

The interlayer structure of the LDHs was also analyzed using X-ray powder diffraction (XRD). We observed that a sharp basal reflection was apparent at a lower 2θ angle and that a non-basal peak was seen at a higher 2θ angle in the diffractograms. The consequent basal spacing was calculated from the sharp peak (0 0 3), which was 8.1 \AA in the case of N-LDH. For DFP-LDH, the peaks of (0 0 6) and (0 0 9) disappeared, which was similarly observed for N-LDH (Fig. S2). With the addition of DFP, the N-LDH lost its original structure. The basal spacing for DFP-LDH was 6.1 \AA , as calculated from the (0 0 3) peak. The distance between the interlayer nitrate ions was 4.1 nm in N-LDH and 3.7 nm in DFP-LDH. The PiP-LDH diffraction peaks did not follow the same pattern as N-LDH. Consequently, the addition of PiP resulted in a mixed structure of aluminum, magnesium, oxygen, hydroxide, and nitrate (Fig. S2).

XPS determined the chemical state and composition of the three LDHs. XPS analysis was performed to study the elemental chemicals' valence states, which provide a measurement of the binding energies (BE) of the core electrons. These undergo a chemical shift after adsorption (Hayez, 2004). Initially, the analysis revealed that the LDHs were comprised of the elements magnesium, aluminum, carbon, oxygen, and nitrogen.

In the pre-adsorption phase, a high-resolution spectrum of Cl_{2p} showed no peak of perchlorate ions (Fig. S3).

The FTIR patterns of all three LDHs before adsorption are shown in Fig. S4. The absorption spectra of three LDHs show the existence of peaks between 3400 cm^{-1} and 3500 cm^{-1} , indicative of the hydrogen bond's stretching vibrations of the hydroxide group in the LDH's layer (Ferreira et al., 2006; Wang et al., 2013). A band's presence near 1600 cm^{-1} in all LDH's spectra was of low intensity, suggestive of the bending vibration of the water molecules (Wu et al., 2010; Guo et al., 2012). Other bands observed near 13000 cm^{-1} were attributed to nitrate ions in all three LDH's interlayer. Lattice vibrational bands were evident between 600 cm^{-1} and 400 cm^{-1} . These were ascribed to magnesium and aluminum ions. The band on the PiP-LDH spectrum located at the wavelength of 1700 cm^{-1} arising from the C=O anhydride was related to the PiP (pinus powder). On the DFP-LDH spectra, the peaks appearing at 1488.1 cm^{-1} , 1270.6 cm^{-1} , and 1048.7 cm^{-1} , representing methylene, C—O—H, and C—OH stretches, respectively, were related to the contents of DFP. On the N-LDH spectra, the peak near 1700 cm^{-1} could be caused by OH stretching.

The observed pH_{pzc} values of the PiP, DFP LDH, were close to 6.2, and the value of N-LDH was 7.1. The pH_{pzc} values provide an understanding of the LDH's surface behavior at different initial-pH values, which is closely related to the sorption of negatively charged perchlorate-anions.

3.2. Adsorption kinetics and isotherm study

We employed two kinetic models describing the experimental data of perchlorate adsorption. The kinetic study was carried out with an initial concentration of 100 mgL^{-1} and 0.1 g of adsorbent. We used this concentration and amount of adsorbent in the kinetic studies for all three LDHs and observed increased adsorption in the initial stages. The reaction reached equilibrium in 20 min, 40 min and two hours for PiP-LDH, DFP-LDH and N-LDH, respectively (Table 1, Fig. S5).

A previous study established that it took six h to reach equilibrium using 1 g C-LDH, and the rate of removal was up to 95% (Wu et al., 2010). Similarly, another study reported a perchlorate removal rate of 85% using organosilica and organoclays over an equilibrium time of 2 h (Seliem et al., 2013). Another group reported 90% perchlorate removal with the use of 0.82 g montmorillonite modified with hexadecyl pyridinium chloride (Makita et al., 2014). Keeping in view the fact that the conditions in the above-discussed studies were the same, the removal rates in our study were 97% with PiP-LDH and 93% with DFP-LDHs, using 0.1 g adsorbent. These rates are comparatively higher than those reported in the previous studies. The adsorbent modified in this study (PiP-LDH and DFP-LDH) did not require acidic, thermal, or any other activation treatment before use, showing the cost- and time-effective materials. The study demonstrates the potential of natural materials such as PiP and DFP to enhance the adsorption of undesired pollutants from contaminated aqueous media within the shortest possible time.

In this study, the correlation coefficient of pseudo-second-order was higher than pseudo-first-order for all three LDHs (Fig. S6). Likewise, the calculated and experimental values of adsorption at the equilibrium state, also concurred with

Table 1 Regression coefficient and kinetic constants of different models.

Kinetic models	Model parameters	N-LDH	PiP-LDH	DFP-LDH
1st Order	$q_{e, \text{exp}}$ (mgg^{-1})	35.1	40	37
	$q_{e, \text{cal}}$ (mgg^{-1})	22	34.4	32.1
	R^2	0.68	0.78	0.85
	k_1 (1/min)	2.6	0.02	2.3
2nd Order	$q_{e, \text{exp}}$ (mgg^{-1})	35.1	40.1	37
	$q_{e, \text{cal}}$ (mgg^{-1})	35	39.02	37
	R^2	0.97	0.98	0.99
	k_2	0.01	0.01	0.04
	h	11.1	13	12.5
Intra particle diffusion model	R_1^2	0.94	0.96	0.95
	R_2^2	0.93	0.95	0.93
	k_{i1} ($\text{mgg}^{-1} \text{min}^{-0.5}$)	0.4	0.4	0.9
	k_{i2} ($\text{mgg}^{-1} \text{min}^{-0.5}$)	0.1	0.1	0.1
	C_{i1} (mgg^{-1})	34	35	30
	C_{i2} (mgg^{-1})	25	39	33

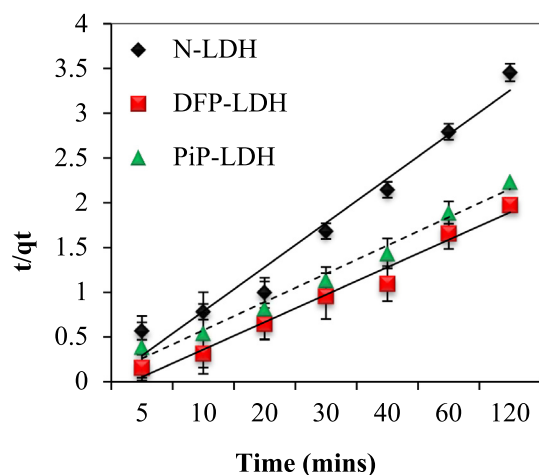
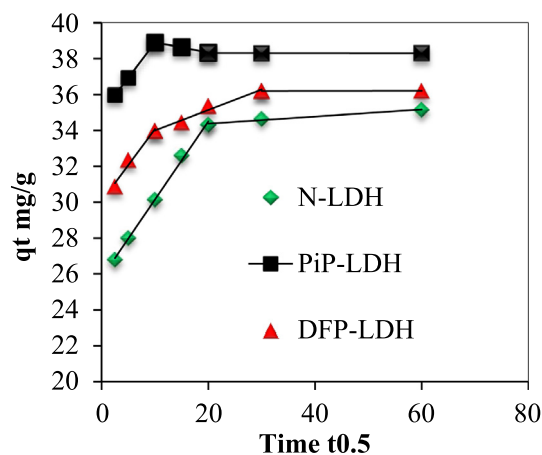
Table 2 Parameters of thermodynamic studies.

LDHs	Temperature (K)					ΔH (kJ mol^{-1})	ΔS ($\text{JK}^{-1}\text{mol}^{-1}$)
	293	298	303	313	323		
N-LDH ΔG°	-852	-904	-1040	-1431	-1613	0.7	3
PiP-LDH ΔG°	-5286	-5648	-6449	-8067	-8835	2.3	2
DFP-LDH ΔG°	-4143	-2477	-1461	-1014	-671	2.8	15

pseudo-second-order as summarized in Table 1, Fig. 1, indicating the suitability of pseudo-second-order in fitting the model. The models suggest that physicochemical interactions are behind the sorption of perchlorate in the case of all the LDHs prepared in this study. The notion is supported by rate constants (k_2), which were proportional to the rate of sorption. The rate constant is determined theoretically by the attributes of the given sorbate for a certain sorbent (Dai et al., 2013). The increase in the number of available sorption sites enabled the

LDH's interaction with the contaminant, via electrostatic interaction (Wang and Shih, 2011).

The intra-particle diffusion model (Fig. 2, Table 1) suggested that if the sorption occurred via intra-particle diffusion, then plot q_t vs. $t^{0.5}$ should be linear; consequently, if the intra-particle diffusion is a rate-determining step, then the plot passes through the origin. We observed a multi-linear graph, suggestive of more than one step, controlling mechanism, for example, surface sorption and chemisorptions

**Fig. 1** Pseudo 2nd order model of N, DFP, and PiP-LDHs.**Fig. 2** Intra-particle diffusion models of N, PiP, and DFP-LDHs.

(Zhihao et al., 2017). It appears that sorption occurred in three steps in the cases of PiP-LDH and DFP-LDH and two for that of N-LDH. The first phase in the cases of PiP-LDH- and DFP-LDH-based sorption was surface adsorption, followed by the gradual sorption of perchlorate, in which case, the intra-particle diffusion within the pores was a rate-determining step. During the third phase of adsorption, the mechanism neared equilibrium. Similarly, the two phases of adsorption by N-LDH were surface adsorption, followed by chemisorption. The plot does not pass through the origin, suggesting that intra-particle diffusion was not a rate-determining step. Therefore, both external and intra-particle diffusion could be rate-determining steps; however, only one of them dominates at any particular time (Zhihao et al., 2017). The enormous value of the surface diffusion constant values (C_s) indicates the surface diffusion playing along compared to intra-particle diffusion as a rate-determining step during sorption (Table 1).

We tested the adsorption isotherms using the Langmuir and Freundlich models. The Langmuir model assumes constant adsorption energy during the reaction and that the adsorption takes place without any interactions between the adsorbate molecules. Also, the Langmuir model asserts that maximized adsorption occurs when the adsorbate's monolayer covers the surface (Shaban et al., 2018). Meanwhile, the Freundlich model supposes that the reaction is homogenous, and the increased uptake capacity results in an exponentially reduced surface binding energy. This energy forms the multilayer from the adsorbed ions (Bagherifam et al., 2014). The results of our study were in favor of the Freundlich isotherm model for describing the adsorption pattern of the LDHs, which was evidenced by the correlation coefficient values being higher than those of the Langmuir model (Table S2, Fig. 3). The calculated values of the Freundlich constant 'n' were 1, 1.8, and 1.5 for PiP, DFP, and N-LDHs, respectively. These are within the range of 1 to 10, suggesting a reasonable adsorption rate, which our results also showed. A value higher than 1 suggests a physical process, while the ' $1/n$ ' < 1 showed that the higher strength and adsorptive capacity of the adsorbent (i.e., LDH). In the case of ' $1/n$ ' > 1, the absorption coefficient increases with the rising concentration

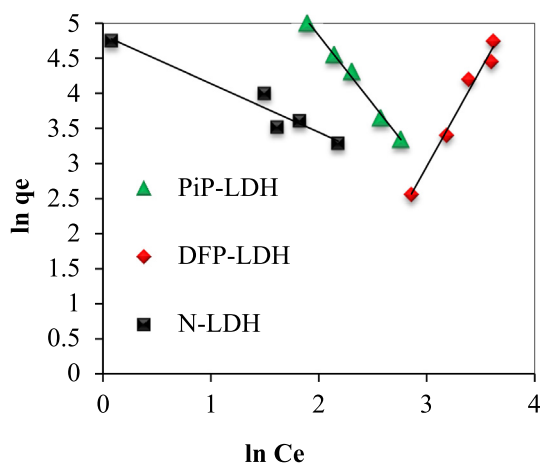


Fig. 3 Freundlich isotherm model of LDHs.

of the solution, leading to an increased hydrophobic surface characterization (Zhang et al., 2015; Ravi, 2014). The maximum adsorption capacity provided by the Langmuir model was 909 mgg^{-1} for PiP, 771 mgg^{-1} for DFP, and 246 mgg^{-1} for N-LDH, indicating PiP-LDH's highest adsorption capacity among three LDHs (Table S2, Fig. S7). The maximum sorption capacity of the PiP-LDH and DFP-LDH is much higher than that of powder activated carbon and anion exchange resin and usually much higher than conventional mesoporous mineral adsorbents, such as activated alumina, silica, zeolite, and montmorillonite (Yu et al., 2009). The current method provides a promising treatment of perchlorate contaminated water, especially at high contamination levels. The perchlorate distribution density on the LDH's surface was indicative of the uptake capacity. The highest distribution density of perchlorate molecules on the LDH-surfaces can be calculated from the maximum sorption capacity and the BET surface area, based on the surface monolayer adsorption from the Langmuir model. Thus the highest numbers of perchlorate molecules per $\text{m}^2 \text{ g}^{-1}$ of LDH surface area (BET) were 209.30, 138.7, and 110.30 for the PiP-, DFP- and N-LDHs, respectively. Since the molecular radius of perchlorate ions is relatively large ($\sim 2.4 \text{ \AA}$), the exceptionally high distribution density of perchlorate molecules in the PiP and DFP-LDH were suggestive of the perchlorate anions sorption by two LDHs, by a process facilitated by interlayer anion exchange rather than surface adsorption.

3.3. Factors affecting adsorption

3.3.1. Effect of pH

The removal efficacy of both PiP-LDH and DFP-LDH increases below the pzc, and maximum adsorption was seen at pH six and after that declined (between 7 and 12) (Fig. S9). A similar increase was observed with N-LDH; however, the maximum adsorption occurred at pH 7. At low pzc value, the surface is supposedly positively charged, and the electrostatic attraction between the LDH surface and the perchlorate anion is stronger, indicating increased adsorption. Above the pzc value, the LDH's surface becomes highly negatively charged, repelling negatively charged perchlorate ions, consequently, decreasing the sorption (Mandal and Mayadevi, 2008). The sorption-facilitating perchlorate removal was due to hydrogen bonding between the hydroxyl (OH^-) ions of LDHs and the electronegative (oxygen) atoms of PFOA. The same occurs between the metal ions (Mg-Al) of LDHs and perchlorate anions. The results were, therefore, suggestive of pH-depending perchlorate-sorption by the LDHs. The observed phenomenon was also affected by the background electrolyte concentration; in which case, a higher background electrolyte concentration spurred a decreased perchlorate sorption. The perchlorate-surface electrostatic attraction plays a dominant role in these conditions. As the higher background concentration increases, OH^- ionic strength also increases and reduces perchlorate sorption, as the electrostatic interaction is also reduced. Under more alkaline conditions, the surface is more negatively charged and caused the electrostatic repulsion between the anionic surface and perchlorate anions, as well as between adjacent perchlorate anions, render decline in the overall process of sorption (Liang et al., 2013; Tang et al., 2010).

3.3.2. Effect of co-existing anions

Perchlorate-contaminated wastewater contains numerous anions such as nitrate (NO_3^-), sulfate (SO_4^{2-}), and phosphate (PO_4^{3-}). The coexisting ions are likely to compete with perchlorate for the available sites on LDHs. The anions, possessing higher negative valence, are prone to exhibit a higher degree of adverse impact on the LDH's adsorption. These ions also interact with the positively charged hydroxide sheets in LDHs, leading to a faster replacement rate (Kwak et al., 2012). The perchlorate's adsorption decreased with increasing coexisting ion concentration (0.1–1 mM; see (Fig. S10)). The anionic effect was greatest for phosphate and then sulfate and, lastly, nitrate. This shows that multivalent anions are adsorbed more readily than monovalent anions due to the increase in the charge radius values occurring in the order mentioned above. Consequently, the nitrate did not have much effect. This phenomenon was observed with all three LDHs.

3.3.3. Effect of temperature

We evaluated the impact of temperature on the adsorption efficacy of the synthesized LDHs using an initial concentration of 100 mg g^{-1} . A temperature range of 20–50 °C was chosen. The adsorption rate showed little variation over the selected range. However, DFP-LDHs experienced a dramatic rise in the adsorption rate at 25 °C. It remained steady and the highest among all three LDHs across the temperature range (Fig. 4). Adsorption, in the case of N-LDH and PiP-LDH peaked at approximately 30 °C and remained steady. The PiP-LDH had a higher adsorption rate than N-LDH, although their patterns were similar. The results showed that a favorable temperature range for adsorption is between 30 °C and 50 °C. Warmer temperatures are considered to enlarge pores and increase activation of the adsorbent surface. Over 30 °C, the adsorbent surface was likely to be at capacity or overcrowded by perchlorate ions, hence the steady rate of adsorption.

3.4. LDH's dose and perchlorate uptake

In general, the use of LDHs, prepared in this study, prompted perchlorate removal that spiked from 0.025 g to 3 g, which

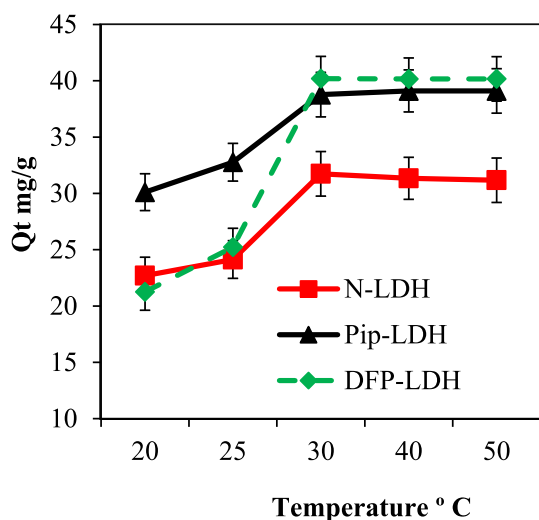


Fig. 4 Temperature effecting perchlorate adsorption by LDHs.

were indicative of more active sites on the surface of LDHs (Fig. S11). In a batch adsorption system, an optimum dose of certain adsorbent is required to cut the cost; we, therefore, used an adsorbent dose of 0.1 g L^{-1} . According to the heterogeneity model, the spectrum of binding energy renders all the sites completely exposed, resulting in high surface adsorption, which is composed of active energy sites at low doses. On the contrary, the high adsorbent dose reduces the availability of higher energy sites, resulting in lowered adsorption capacity (Fleutot et al., 2012).

It was observed that increasing the dose from 0.025 g to 3 g, also increases the removal percentage of perchlorate by all LDHs, for there were more active sites on the surface of LDHs. Uptake capacities of LDHs decreases as the concentration of dose increases 0.025 g to 3 g. In a batch adsorption system, applying an optimum dose of suitable adsorbent is required to reduce the treatment cost in all subsequent tests; therefore, an adsorbent dose of 0.1 g L^{-1} was used. According to the heterogeneity model, the surface is composed of active energy sites, since at low doses, the spectrum of binding energy renders all the sites completely exposed, resulting in high surface adsorption (Pavlovic et al., 2009). Likewise, at high adsorbent doses, the availability of higher energy sites decrease, resulting in lowered adsorption capacity (Fig. S11) Fleutot et al. (2012).

3.5. SEM image analysis of LDHs

SEM images were taken of all three LDHs, revealing the surfaces of the LDH material pre- and post-adsorption. The pre-adsorption surface of N-LDH appeared to consist of thick massive particles and an agglomerated state of particles, due to retained water molecules (Fig. 5-a). The pre-adsorption image of PiP-LDH showed a loosely bound particle structure, in which rod-like structures were embedded in the LDH, comprising of PiP (Fig. 5-b). The pre-adsorption surface of DFP-LDH was rough and compact, with the coalescence of powdery particle-like appearance. Its structural appearance was quite distinct from other LDHs (Fig. 5-c). In post-adsorption SEM images, N-LDH appeared as a tightly bound material, attributed to the adsorption of perchlorate ions. In the energy-dispersive X-ray spectroscopy (EDS) images, red-dotted particles represent the perchlorate ion adsorption. The post-adsorption image was also taken, the analysis showed that the compact and robust structure, and previously observed rod-like structures, had disappeared, which was likely a result of perchlorate embedding into the LDH structure. After the adsorption of perchlorate by DFP-LDH, the structure in the image appeared smooth and homogenous, and this is likely to be a consequence of perchlorate adsorption. The red particles in the EDS image represent chlorine and therefore show the presence of perchlorate in the structure of DFP-LDH, pinpointing the adsorption site (Fig. 5-a, b, c).

3.6. Post adsorption analysis

The mechanistic insight into perchlorate adsorption by LDHs was gained from post-adsorption characteristic XRD diffractograms (Fig. S12). XRD showed that the basal d-spacing of N-LDH changed slightly from 8.1 \AA to 8.0 \AA . For DFP-LDH, it shifted from 6.1 \AA to 4.1 \AA . The observed d-spacing changes could be explained by anion exchange and the recon-

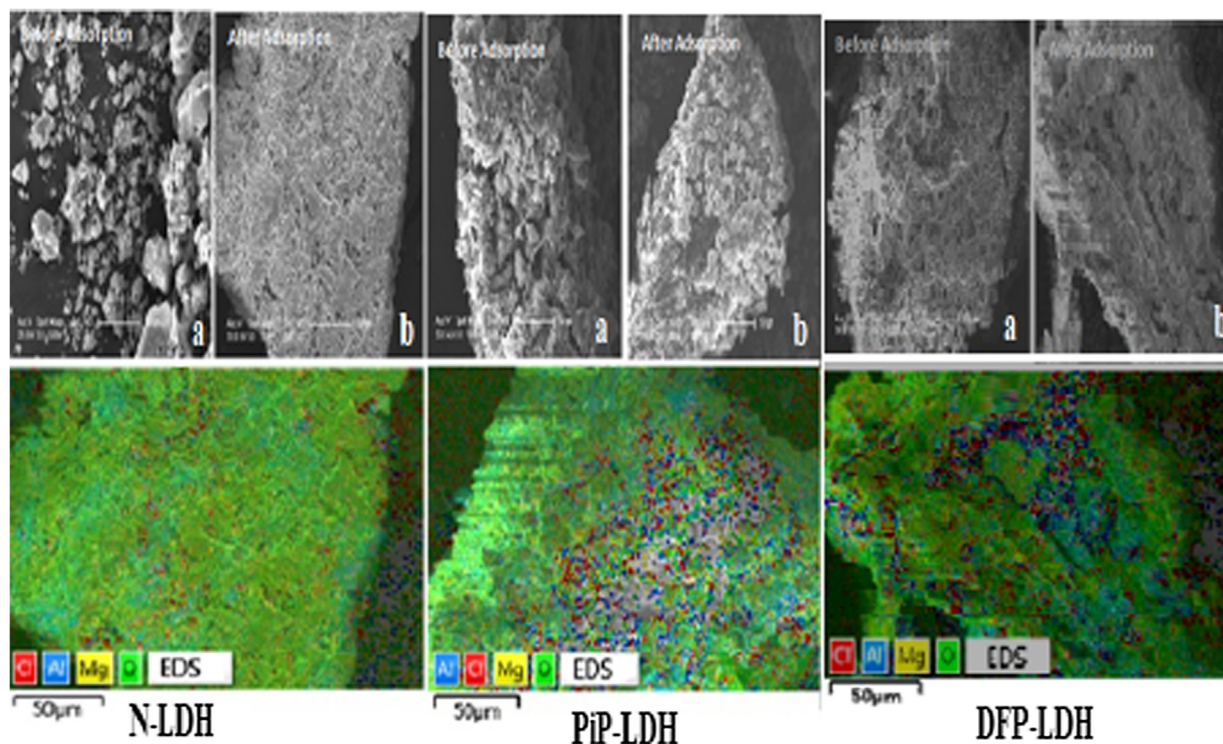


Fig. 5 SEM images revealing (a) pre-adsorption and (b) post-adsorption states of LDHs.

struction of the layer structure as the nitrate ions were replaced by perchlorate ions (Grover et al., 2009). Since the interlayer spacing in N-LDH decreased from 4.1 nm to 4 nm, and from 3.8 nm to 2.2 nm in DFP-LDH, the cause is likely to be ion exchange (Lv et al., 2006). Furthermore, the lessening intensity of nitrate peaks after adsorption indicated the perchlorate-LDH intercalation ion exchange is likely to have changed the charge density (Halajnia et al., 2013; Yang et al., 2014; Hu et al., 2017). PiP-LDH behaves differently after adsorption: the rebuilt PiP-LDH's structure was similar to the rebuilt structure of N-LDH. Furthermore, the structural changes in PiP-LDH following adsorption were confirmed by FTIR spectra, revealing a perchlorate peak. The FTIR and XPS diffractograms also suggested that perchlorate replaced nitrate ions between the PiP-LDH's layers. In FTIR, the peak related to nitrate disappeared after adsorption, suggesting anion exchange.

Post-adsorption XPS analysis (Fig. S13) revealed a high-resolution spectrum of PiP-LDH, deconvoluted into peaks with BEs at 209.3 and 209.1 eV, which confirmed perchlorate adsorption into the LDH interlayer. The peak visualized in DFP-LDH's spectrum at BE of 208.9 eV corresponds with perchlorate adsorption. The peaks centered at BE of 209 eV in the N-LDH's spectrum were also indicative of perchlorate surface adsorption on the LDH surface. That the elements magnesium, aluminum, oxygen, and carbon were involved in surface complexation with perchlorate was evident from the binding energy changes summarized in Table S3. The BEs of C_{1s} , N_{1s} , Mg_{2p} , Al_{2p} , O_{1s} showed they increased after adsorption, which increased with perchlorate adsorption. The elements mentioned above densities decreased, and BE increased due to the higher electronegativity of the perchlorate ions. The phenomenon is indicative of LDH's role in perchlorate surface adsorption (Hudcov et al., 2018). This was also observed in the

FTIR spectral analysis, where perchlorate was adsorbed on the surface through hydrogen bonding and anion exchange.

FTIR analyses showed that adsorption changed the peak position on the LDHs' FTIR spectra (Fig. 6). The peaks located at 3400 cm^{-1} and 1600 cm^{-1} shifted for all three LDHs following the perchlorate adsorption. The peaks shift to a higher wavelength, indicating weak hydrogen bonding between perchlorate and hydrogen ions. Conversely, those shifting towards a lower wavelength suggested strong hydrogen bonding between pollutants and the LDH. Currently, the PiP-LDH spectra revealed perchlorate adsorption, while the peaks at 788.8 cm^{-1} and 554 cm^{-1} were ascribed to $M-ClO_4^- - M$ interactions or lattice vibrations. The peaks at 1788.6 and 1559.6 disappear after adsorption, indicating perchlorate adsorption in PiP (Wu et al., 2013). In DFP-LDH, the stronger perchlorate adsorption peak appeared at 1101.5 cm^{-1} , and 1781.9 cm^{-1} indicated bonding between ClO_4^- and LDH. For N-LDH, the perchlorate adsorption peaks were apparent at 781 cm^{-1} and 554.5 cm^{-1} because of the M -pollutant- M interaction. In N-LDH, individual bonds shifted to higher frequencies, suggestive of weak hydrogen bonding occurring in this layer. The shift in OH^- peaks was likely nudged by electrostatic interaction, for example, hydrogen bonding between LDHs and perchlorate. The peak near 1300 cm^{-1} was related to nitrate ions disappearing in all three LDHs after perchlorate adsorption, indicating anion exchange.

3.7. Mechanistic insight

In general, the ion exchange and surface adsorption facilitated the perchlorate adsorption by DFP-LDH, while that by N-LDH was apparently facilitated by electrostatic interaction. These interactions were confirmed by the results of the FTIR,

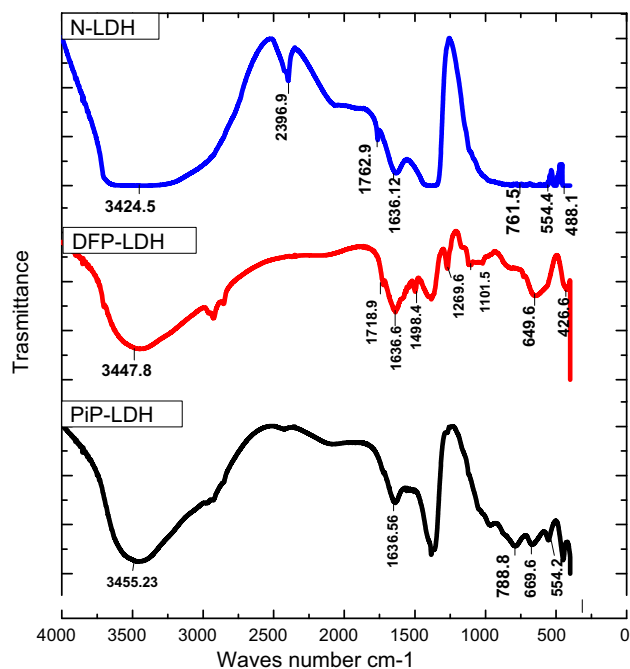


Fig. 6 FTIR-spectra of LDHs revealing a shift in peak position post-adsorption stage.

XPS, and XRD analyses. Adding DFP to N-LDH induced certain structural modifications as evinced by the XRD spectra, for example, this disappearance of diffraction peaks (0 0 9) and (0 0 6) (Fig. S2). The FTIR revealed that after the addition of DFP, there was an increase in the active sites for adsorption. The peaks related to DFP-LDH, appearing at 1488.1 cm^{-1} and 1270.6 cm^{-1} , shrunk after adsorption at wavelengths of 1408.4 cm^{-1} and 1269.4 cm^{-1} , respectively, indicating adsorption of perchlorate on DFP via strong hydrogen bonding. Another peak located at 1048.7 cm^{-1} disappeared after adsorption, indicating perchlorate adsorption around C—OH (Fig. S4). Furthermore, anion exchange occurred between nitrate ions and perchlorate ions, as seen in XRD analysis, where interlayer distance decreases as a result of perchlorate adsorption. The adsorption was also confirmed from FTIR spectra, revealing the disappearance of the nitrate peaks (Fig. S2).

In the case of PiP-LDH-based adsorption, a ‘rebuilding’ mechanism was involved, similar to the memory effect of C-LDH, in which CO_3^{2-} used as the interlayer in LDH (Gao et al., 2018). It disappeared after calcinated/thermal treatment and formed a mixed structure. It regained its structure after adsorption. In our study, nitrate ions were used as an interlayer anion. After the addition of PiP, a mixed structure of Mg, Al, O, OH, PiP, and NO_3^- formed without requiring any thermal treatment. The XRD spectra revealed (0 0 3), (0 0 6) and (0 0 9) diffraction peaks disappearing in PiP-LDH, which previously appeared in the parent, N-LDH (Fig. S2). In the post-adsorption XRD analysis (Fig. S12), a ‘rebuilt’ structure was seen, akin to N-LDH, except that the nitrate ion was replaced by perchlorate in the interlayer. Furthermore, the FTIR spectra also revealed that nitrate peaks disappeared while perchlorate adsorption peaks appeared via anion exchange. Additionally, a higher degree of anion

exchange was seen with PiP-LDH compared to other LDHs, showing more adsorption capacity of PiP-LDH (Langmuir model; Table S2). Interestingly, nitrate readily exits the structural matrix; in comparison, it probably faces great hindrance when present between the layers. The active sites available to the pollutants increased with the addition of PiP. We noticed that peak at 1788.6 cm^{-1} disappeared, indicating perchlorate adsorption by PiP. Therefore, the addition of PiP and DFP enhances the active sites and, thus, the overall adsorption capacity of LDHs.

4. Conclusions

The study showed that the newly synthesized PiP and DFP-LDHs might be effectively used for perchlorate removal from contaminated wastewater. The shortest equilibrium time observed was 20 m and 40 m with PiP-LDH, followed by DFP-LDH, respectively. The information entailed by the model suggested Physicochemical interactions behind the sorption of perchlorate on all the studied LDHs. The ion exchange and surface adsorption were possible mechanisms behind the adsorption of perchlorate by DFP-LDH and N-LDH, through hydrogen bonding, while the ion exchange and ‘re-built’ mechanisms facilitated perchlorate adsorption by PiP-LDH.

Declaration of Competing Interest

The authors declare that they have no known competing financial interests or personal relationships that could have appeared to influence the work reported in this paper.

Appendix A. Supplementary material

Supplementary data to this article can be found online at <https://doi.org/10.1016/j.arabjc.2020.03.001>.

References

- Bagherifam, S., Komarneni, S., Lakzian, A., Fotovat, A., Khorasani, R., Huang, W., Ma, J., Wang, Y., 2014. Evaluation of Zn-Al-SO₄ layered double hydroxide for the removal of arsenite and arsenate from a simulated soil solution: isotherms and kinetics. *Appl. Clay Sci.* 95, 119–125.
- Bardiya, N., Bae, J.-H., 2011. Dissimilatory perchlorate reduction: a review. *Microbiol. Res.* 166, 237–254.
- Chen, W.F., Cannon, F.S., Mendez, J.R., 2005. Ammonia tailoring of GAC to enhance perchlorate removal. I. Characterization of NH₃ thermally tailored GACs. *Carbon* 43 (3), 573–580.
- Dai, W., Hu, J., Zhou, L.M., Li, S., Hu, X., Huang, H., 2013. Removal of dibenzothiophene with composite adsorbent MOF-5/Cu(I). *Energy Fuels* 27, 816–821.
- Darracq, G., Baron, J., Joyeux, M., 2014. Kinetic and isotherm studies on perchlorate sorption by ion-exchange resins in drinking water treatment. *J. Water Process Eng.* 3, 123e131.
- Debdipta, B., Amit, D., Werner, S.K., Udo, W., Gert, H., 2014. Advances in layered double hydroxide (LDH)-based elastomer composites. *Prog. Polym. Sci.* 39, 594–626.
- Deng, S., Yu, Q., Huang, J., Yu, G., 2010. Removal of perfluorooctane sulfonate from wastewater by anion exchange resins: Effects of resin properties and solution chemistry. *Water Res.* 44, 5188–5195.
- EPA (U.S. Environmental Protection Agency), 1998. Guidelines for Ecological Risk Assessment. EPA/630/R-95/002F. Risk Assessment Forum, U.S. Environmental Protection Agency, Washington,

- DC [online]. Available: <http://cfpub.epa.gov/ncea/cfm/recordisplay.cfm?deid=12460> [accessed June 3, 2007].
- Ferreira, O.P., Moraes, S.G., Durán, N., Cornejo, L., Alves, O.L., 2006. Evaluation of boron removal from water by hydrotalcite-like compounds. *Chemosphere* 62, 80–88.
- Fleutot, S., Dieudonné, B., Dupin, J.C., Renaudin, G., Martinez, H., 2012. Thermal behaviors and grafting process of LDH/benzene derivative hybrid systems. *Thermochim. Acta* 538, 1–8.
- Langmuir 34 (19), 5386–5395. <https://doi.org/10.1021/acs.langmuir.8b00059>.
- Grover, K., Komarneni, S., Katsuki, H., 2009. Uptake of arsenite by synthetic layered double hydroxides. *Water Res.* 43, 3884–3890.
- Gullick, R.W., LeChevallier, M.W., Barhorst, T.S., 2001. Occurrence of perchlorate in drinking water sources. *J. Am. Water Works Assoc.* 93 (1), 66–77.
- Guo, Y., Zhu, Z., Qiu, Y., Zhao, J., 2012. Adsorption of arsenate on Cu/Mg/Fe/La layered double hydroxide from aqueous solutions. *J. Hazard. Mater.* 239, 279–288.
- Halajnia, A., Oustan, S., Najafi, N., Khataee, A.R., Lakzian, A., 2013. *Appl. Clay Sci.* 80–81 (13), 305.
- Hayez, V., 2004. A. Franquet, A. Hubin, H. Terryn, *Surf. Interf. Anal.* 36, 876.
- Hu, Z., Song, X., Wei, C., Liu, J., 2017. Behavior and mechanisms for sorptive removal of perfluorooctane sulfonate by layered double hydroxides. *Chemosphere* 187, 196–205.
- Hudcov, B., Veselsk, V., Filip, J., Cihalov, S., Komarek, M., 2018. Highly effective Zn(II) and Pb(II) removal from aqueous solutions using Mg-Fe layered double hydroxides: Comprehensive adsorption modeling coupled with solid state analyses. *J. Cleaner Prod.* 171, 944–953.
- Kwak, N.S., H.M. Park, T.S., 2012. Hwang, *Chem. Eng. J.* 191, 579–587.
- Liang, Zang, Y., Xu, Y., Tan, X., Houe, W., Wangb, L., Sun, Y., 2013. *Colloids Surf. A: Physicochem. Eng. Aspects* 433, 122–131.
- Lin, Y., Fang, Q., Chen, B., 2014. Perchlorate uptake and molecular mechanisms by magnesium/aluminum carbonate layered double hydroxides and the calcined layered double hydroxides. *Chem. Eng. J.* 237, 38–46.
- Lv, L., He, J., Wei, M., Evans, D.G., Duan, X., 2006. Uptake of chloride ion from aqueous solution by calcined layered double hydroxides: equilibrium and kinetic studies. *Water Res.* 40, 735–743.
- Makita, Y., Chitraker, R., Sonoda, A., 2014. Removal of perchlorate ion in Tap water with mountmorillonite modified with Hexadecylpyridinium chloride. *J. Ion Exchange.* 25 (4), 184–190.
- Mandal, S., Mayadevi, S., 2008. Cellulose supported layered double hydroxides for the adsorption of fluoride from aqueous solution. *Chemosphere* 72 (6), 995–998.
- Park, J.Y., Kim, J.H., 2011. Characterization of adsorbed arsenate on amorphous and nano crystalline MgFe-layered double hydroxides. *Nanopart. Res.* 13, 887–894.
- Pavlovic, I., Pérez, M.R., Barriga, C., Ulibarri, M.A., 2009. *Appl. Clay Sci.* 43, 125–129.
- Ravi, S.M., 2014. Selvaraj. *Dalton Trans.* 43, 5299–5308.
- Rouquerol, J., Avnir, D., Fairbridge, C.W., Everett, D.H., Haynes, J. H., Pernicone, N., Ramsay, J.D.F., Sing, K.S.W., Unger, K.K., 1994. Recommendations for the characterization of porous solids. *Pure & Appl. Chem.* 66 (8), 1739–1758. ISSN electronic 1365-3075.
- Seliem, M.K., Komarneni, S., Byrne, T., Cannon, F.S., Shahien, M. G., Khalil, A.A., Abd El-Gaid, I.M., 2013. Removal of perchlorate by synthetic organosilicas and organoclay: Kinetics and isotherm studies. *Appl. Clay Sci.* 71, 21–26.
- Shaban, M., Abukhadra, M.R., Rabia, M., Abd Elkader, Y., Abd El-Halim, M.R., 2018. Investigation the adsorption properties of graphene oxide and polyaniline nano/micro structures for efficient removal of toxic Cr(VI) contaminants from aqueous solutions: kinetic and equilibrium studies. *Rend Lincei-Sci. Fis.* 29, 141–154.
- Srinivasan, Thiruvengkatachari, V., 2009. Perchlorate: Health effects and technologies for its removal from water resources. *Int. J. Environ. Res. Public Health* 6 (1419).
- Srivastava, V., Weng, C.H., Singh, V.K., Sharma, Y.C., 2011. Adsorption of nickel ions from aqueous solutions by nano alumina: kinetic, mass transfer, and equilibrium studies. *J. Chem. Eng. Data* 56, 1414e1422.
- Tang, C.Y., Shiang Fu, Q., Gao, D., Criddle, C.S., Leckie, J.O., 2010. Effect of solution chemistry on the adsorption of perfluorooctane sulfonate onto mineral surfaces. *Water Res.* 44, 2654–2662.
- Titulaer, M., Jansen, J., Geus, J., 1994. *Clays Clay Miner.* 42, 249–258.
- Urbansky, E.T., 2002. Perchlorate as an environmental contaminant. *Environ. Sci. Pollut. Res. Int.* 9, 187–192.
- US EPA (United States Environmental Protection Agency), 2014. Technical Fact Sheet e Perchlorate. http://www2.epa.gov/sites/production/files/2014-03/documents/ffrrofactsheet_contaminant_perchlorate_january2014_final.pdf.
- USEPA, 2003. Environmental Protection Agency. Integrated Risk Information System (IRIS). Glossary of Terms. Office of Research and Development. Washington, DC. 2003. Available online: <http://Nwww.US EPA.gov/iris>.
- Wagner, H.P., Pepich, B.V., Pohl, C., Later, D., Joyce, R., Srinivasan, K., Thoams, D., Wagner, H.P., Pepich, B.V., Pohl, C., Later, D., Joyce, R., Srinivasan, K., Thoams, D., Wan, S., Wang, S., Lic, Y., Gao, B., 2017. Functionalizing biochar with Mg–Al and Mg–Fe layered double hydroxides for removal of phosphate from aqueous solutions. *J. Ind. Eng. Chem.* 47, 246–253.
- Wang, Q., O'Hare, D., 2012. Recent advances in the synthesis and application of layered double hydroxide (LDH) nanosheets. *Chem. Rev.* 112, 4124–4155.
- Wang, F., Shih, K., 2011. Adsorption of perfluorooctanesulfonate (PFOS) and perfluorooctanoate (PFOA) on alumina: influence of solution pH and cations. *Water Res.* 45, 2925–2930.
- Wang, G., Yang, M., Li, Z., Lin, K., Jin, Q., Xing, C., Hu, Z., Wang, D., 2013. Synthesis and characterization of Zn-doped MgAl-layered double hydroxide nanoparticles as VC heat stabilizer. *J. Nanopart. Res.* 15, 1882–1890.
- Wendelken, S.C., Vanatta, L.E., Coleman, D.E., Munch, D.J., 2006. Perchlorate in water via US environmental protection agency method 331: determination of method uncertainties, lowest concentration minimum reporting levels, and Hubaux- Vos detection limits in reagent water and simulated drinking water. *J. Chromatogr. A* 1118, 94–99.
- Wilkin, R.T., Fine, D.D., Burnett, N.G., 2007. Perchlorate behavior in municipal lake following fireworks displays. *Environ. Sci. Technol.* 41, 3966–3971.
- Wu, X.L., Tan, X.L., Yang, S.T., Wen, T., Guo, H.L., Wang, X.K., Xu, A.W., 2013. Coexistence of adsorption and coagulation processes of both arsenate and NOM from contaminated groundwater by nano-crystallined Mg/Al layered double hydroxides. *Water. Res.* 47, 4159–4168.
- Wu, X., Wang, Y., Xu, L., Lv, L., 2010. Removal of perchlorate contaminants by calcined Zn/Al layered double hydroxides: Equilibrium, kinetics, and column studies. *Desalination* 256, 136–140.
- Yang, L.G., Yan, Y.M., Yan, S.J.Yu., Shan, R.R., Yu, H.Q., Zhu, B. C., Du, B., 2014. *Sep. Purif. Technol.* 124, 36–42.
- Yu, Q., Zhang, R., Deng, S., Huang, J., Yu, G., 2009. Sorption of perfluorooctane sulfonate and perfluorooctanoate on activated carbons and resin: kinetic and isotherm study. *Water Res.* 43, 1150e1158.
- Zhang, F., Du, N., Li, H., Song, S., Hou, W., 2015. *Colloid Polym. Sci.* 293, 1961–1969.
- Zhihao, H., Xin, S., Changlong, W., Jianguo, L., 2017. Behavior and mechanisms for sorptive removal of perfluorooctane sulfonate by layered double hydroxides. *J. Chemosphere* 187, 196–205.